Electronic Supplementary Material (ESI) for Nanoscale.

Plasmonic Photocatalysis in Aqueous Solution: Assessing the Contribution of Thermal Effects and Evaluating the Role of Photogenerated ROS

Yoel Negrín-Montecelo,[1,2] Charlène Brissaud,[3] Jean-Yves Piquemal,[3] Alexander O. Govorov,[4] Miguel A. Correa-Duarte,[1,2] Lucas V. Besteiro,[1,2,*] and Miguel Comesaña-Hermo[3,*]

[1]CINBIO, Universidade de Vigo, Department of Physical Chemistry, 36310 Vigo, Spain

[2]Galicia Sur Health Research Institute (IISGS), CIBERSAM, 36310 Vigo, Spain

[3]Université Paris Cité, CNRS, ITODYS, Paris F-75013 Paris, France

[4]Department of Physics and Astronomy, Ohio University, Athens, Ohio 45701, United States

lucas.v.besteiro@uvigo.es; miguel.comesana-hermo@u-paris.fr

Materials: Tetrachloroauric acid ($HAuCl_4 \cdot 3H_2O$), hexadecyltrimethylammonium bromide (CTAB), sodium borohydride ($NaBH_4$), hydrochloric acid (HCl), L-ascorbic acid (AA), poly(allylamine hydrochloride) (PAH, MW: 17500 g/mol), sodium chloride (NaCl), poly(styrenesulfonate) (PSS, MW: 14900 g/mol), tetraethylorthosilicate 98% (TEOS), tertbutanol (tBuOH), isopropanol (iPrOH), sodium hydroxide (NaOH), terephthalic acid (TPA), 1,3-diphenylisobenzofuran (DPBF), 9,10-anthracenediyl-bis(methylene) dimalonic acid (ABDA), dimethyl sulfoxide (DMSO), pentafluorobenzenesulfonyl fluorescein (PBSF), nitro blue tetrazolium chloride 90% (NBT), rhodamine B (RhB), ammonium hydroxide solution 28−30% (NH_4OH) and sodium citrate ($Na_3C_6H_5O_7$) were purchased from Sigma-Aldrich. Pentafluorobenzenesulfonyl fluorescein (PBSF) was purchased from Santa Cruz Biotechnology. TiO_2 nanoparticles of 5 nm were purchased from Nanoamor. Pure grade ethanol and Milli-Q grade water were used in all preparations.

Synthesis and functionalization of silica beads: Monodisperse silica spheres (502 (±19) nm) were prepared using a modified Stöber method.[1] Typically, a TEOS solution (1.7 mL, 1.2 M) was added to a solution containing ethanol (18.12 mL), ammonium hydroxide (1.96 mL), and water (3.21 mL). This mixture was stirred at room temperature for 2 h. The excess of reagents was removed by three centrifugation-redispersion cycles with ethanol and water (5000 rpm, 30 min).

Subsequently, PAH was dissolved in a 0.5 M NaCl aqueous solution (pH 5.0) with a final polymer concentration of 1 mg/mL. Then, 25 mL of the positively charged PAH solution were added to the silica nanoparticles (20 mg dispersed in 20 mL of water) and stirred at room temperature for 30 min. The excess of reagents was removed by three centrifugation-redispersion cycles with water (5000 rpm, 30 min).

Synthesis of gold nanorods (Au NRs) and PSS coating: Au NRs with localized surface plasmon resonance (LSPR) centered at 818 nm were synthesized by the seed-mediated growth method as described elsewhere.[2] The dimensions obtained from TEM were 53 (±5) nm of length and 13 (±1) nm of thickness (aspect ratio 4.05). The Au NRs were subsequently coated with a layer of a negatively charged polyelectrolyte (PSS) in order to proceed to the deposition onto the positively charged PAH functionalized silica beads.[3]

Addition of AuNRs@PSS onto functionalized silica beads. 1 mL of AuNRs@PSS (0.5 mM) were added to 5 mg of functionalized silica NPs dispersed in 5 mL of water (100 nmol of metal per mg of SiO_2). The mixture

was stirred at room temperature for 3 h and washed by three centrifugation-redispersion cycles (6000 rpm, 30 min). The product was redispersed in 5 mL of water.

Deposition of TiO_2. 50 mg of TiO_2 (5 nm) redispersed in 100 mL of a sodium citrate solution (2,5 mM) was sonicated for 1 h with an ultrasonic tip. The aggregates of TiO_2 NPs were removed by centrifugation (3500 rpm, 10 min). Then, 5 mL of the SiO_2@NPs solution coated with another layer of PAH was added to 4 mL of the solution of TiO_2 and stirred at room temperature for 60 min. The excess of TiO_2 was removed by three centrifugation-redispersion cycles (6000 rpm, 30 min). Finally, the product was redispersed in 5 mL of water. The ratio TiO_2/SiO_2 was 2.1 ± 0.09 wt% (ICP analysis).

Structural and optical characterization: TEM images were obtained using a JEOL JEM 1010 transmission electron microscope operating at an acceleration voltage of 100 kV. UV−visible−NIR spectra were obtained with Hewlett-Packard HP8453 and Cary 5000 spectrophotometers.

Photocatalytic studies: All the photocatalytic experiments were performed using 1 mL of the hybrid photocatalysts (1 mg/mL) in an aqueous solution of RhB (10^{-5} M) with a total volume of 5 mL. The mixtures were stirred for 1 h in the dark to blend well and allow the adsorption-desorption equilibrium before the irradiation. After this, 4 mL were introduced in a quartz cell (1 cm path) that was placed inside a controlled water bath at 20 °C under magnetic stirring (1200 rpm). The photocatalytic reaction was followed by measuring the decrease of absorbance of the organic dye (measured at A_{max} = 554 nm). When necessary, Ar was bubbled in the solution before the photocatalytic process. Irradiation source: 150 W SLS401 xenon short-arc light source and a range of 360–2400 nm. Alternatively, LOT solar simulator (300 W Xe lamp) with λ = 350–2400 nm has been also used.

Photocatalytic detection of ROS by selective scavenger chemistry

Detection of OH• by the phototransformation of TPA into 2-HTPA.

8.3 mg of terephthalic acid (TPA) and 8 mg NaOH were dissolved in 100 mL of H_2O (0,5 mM and 2 mM, respectively). 3 mL of this solution was added to 1 mg of the photocatalyst and stirred for 30 min the dark. The mixture was then placed in a 3 mL cuvette inside a controlled water bath at 20 °C under magnetic stirring (1200 rpm) and irradiated for 180 min. Fluorescence measurements every 30 min allowed to characterize the appearance of fluorescence due to the transformation of TPA into 2-HTPA (λ_{exc}: 315 nm, λ_{emm}: 425 nm).[4]

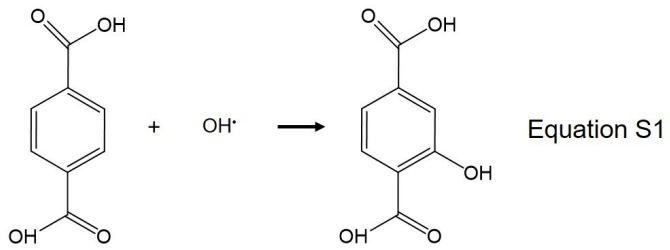

Detection of $^1O_2$ through the phototransformation of ABDA into ABDA-O_2.

9,10-Anthracenediyl-bis(methylene) dimalonic acid (ABDA) (4.1 mg) was dissolved in 10 mL of DMSO (1 mM). 50 µL of this solution was added to 1 mg of catalyst dissolved in 2.95 ml H_2O and stirred for 30 min in the dark. The mixture was then placed in a 3 mL cuvette inside a controlled water bath at 20 °C under magnetic stirring (1200 rpm) and irradiated for 40 min. ROS production was confirmed by absorbance measurements every 10 min to follow the decrease of the signature centered at 399 nm.[5]

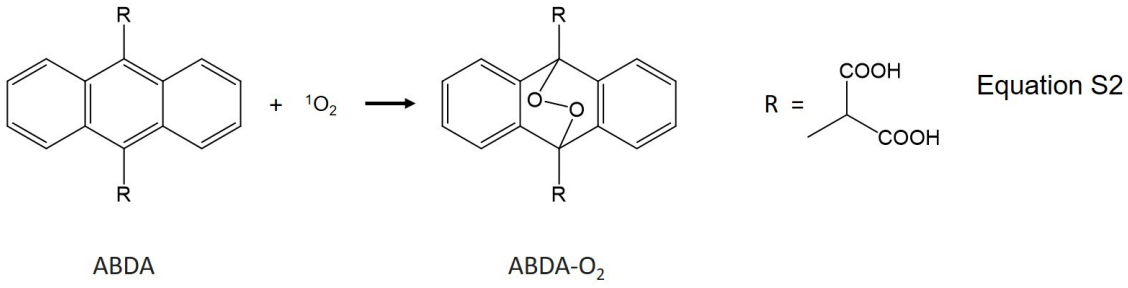

Detection of H_2O_2 through the phototransformation of PBSF into fluorescein.

Pentafluorobenzenesulfonyl fluorescein (PBSF) (1 mg) was dissolved in 1,78 mL of EtOH (1 mM, stored in the dark at -20 °C). 300 µL of this solution were added to 1 mg of catalyst dissolved in 2.7 ml H_2O and stirred for 30 min in the dark. The mixture was then placed in a 3 mL cuvette inside a controlled water bath at 20 °C under magnetic stirring

(1200 rpm) and irradiated for 40 min. ROS production was confirmed by the appearance of fluorescence as a result of the perhydrolysis of PBSF into fluorescein (λ_{exc}: 485 nm, λ_{em}: 522 nm).[4]

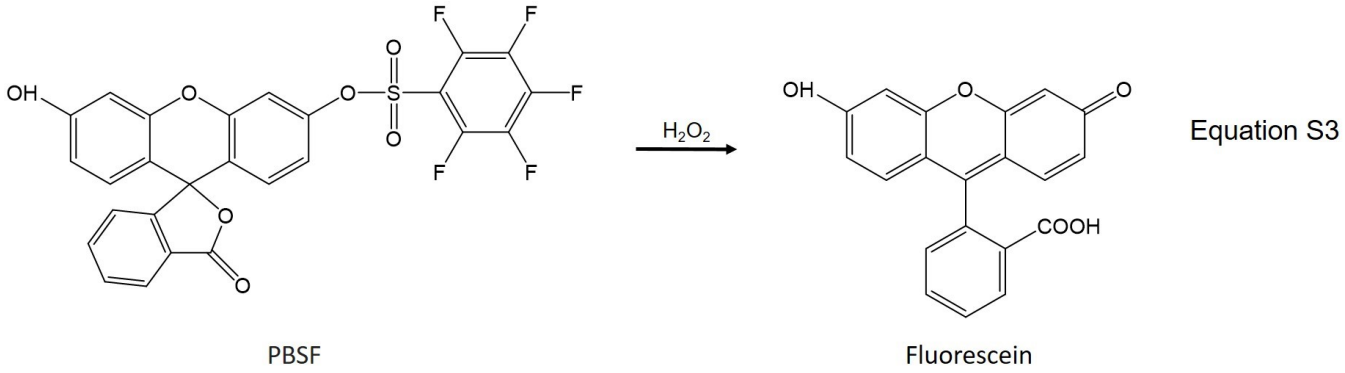

PBSF Fluorescein

Equation S3

Detection of $\bullet O_2^-$ through the phototransformation of NBT into formazan.

2,2′-Di-p-nitrophenyl-5,5′-diphenyl-(3,3′-dimethoxy)-4,4′-bisphenyleneditetrazolium chloride (Nitro Blue tetrazolium, NBT) (9 mg) was dissolved in 10 mL of H_2O (1 mM). 30 µL of this solution were added to 1 mg of catalyst dissolved in 2.97 ml H_2O and stirred for 30 min in the dark. The mixture was then placed in a 3 mL cuvette inside a controlled water bath at 20 °C under magnetic stirring (1200 rpm) and irradiated for 40 min. Absorbance measurements every 5 min allowed to follow the decrease of the signal of NBT (λ_{max}: 256 nm).[6]

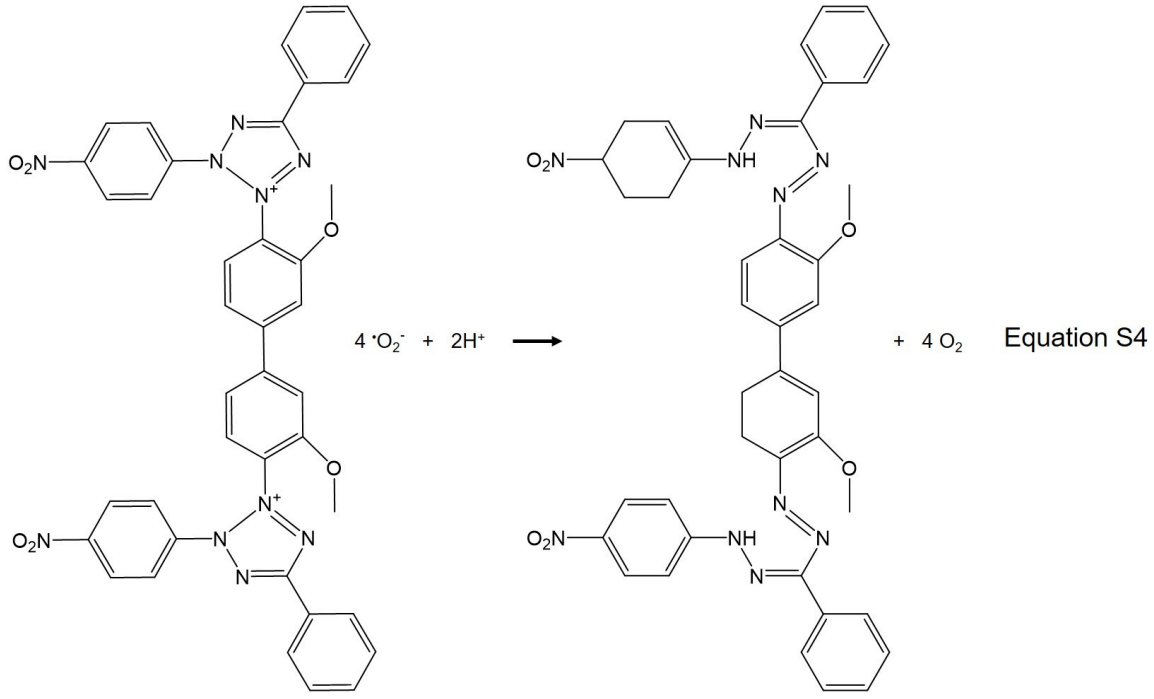

NBT Formazan

Equation S4

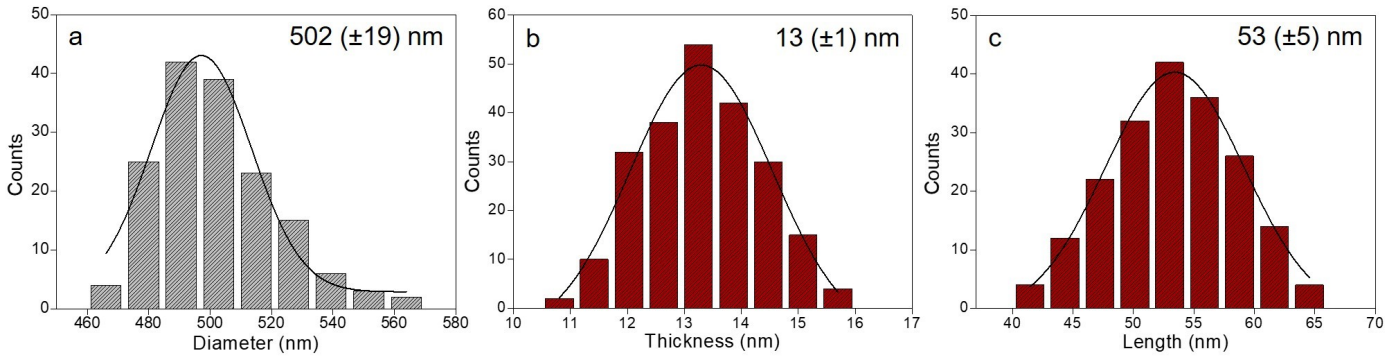

Figure S1. Size histograms for the SiO_2 beads (used as substrates) and the Au NRs. The TiO_2 NPs (5 nm) are provided from Nanoamor.

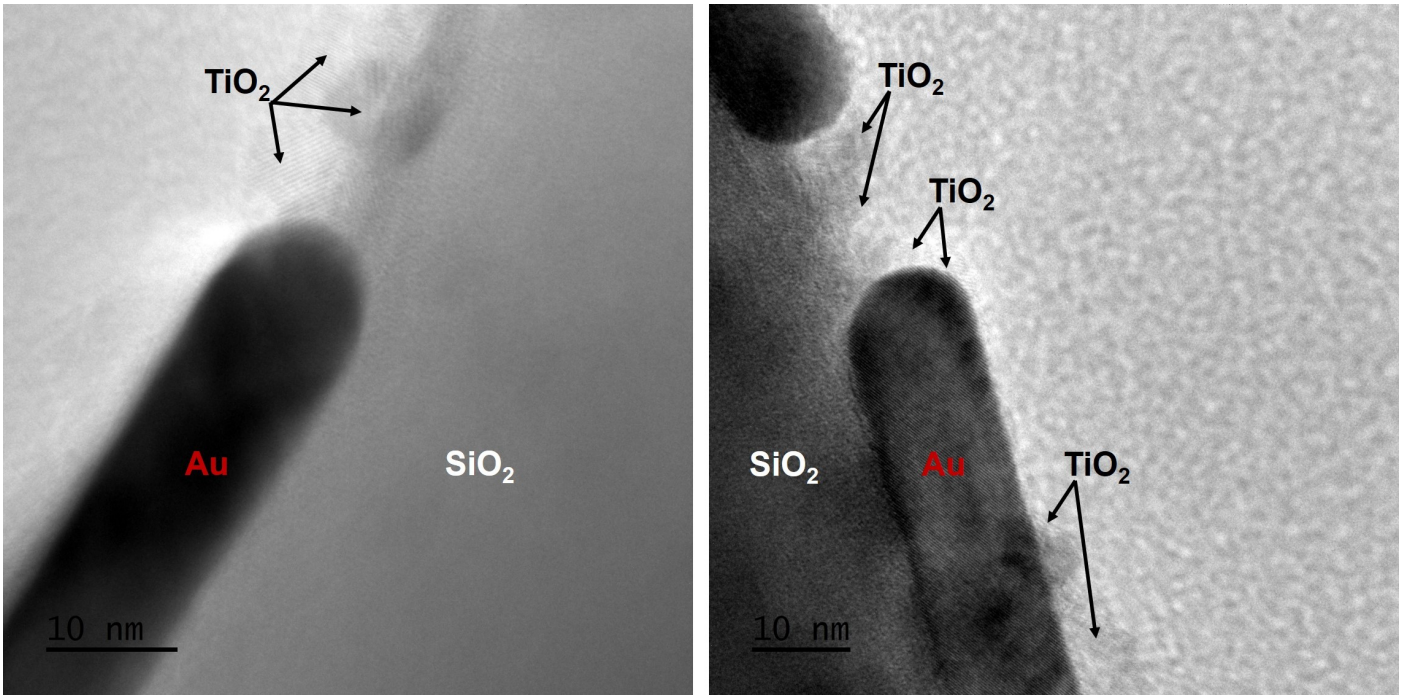

Figure S2. HRTEM images of the SiO_2@AuNR@TiO_2 hybrids in which the physical interface between the metal and semiconductor components can be clearly observed.

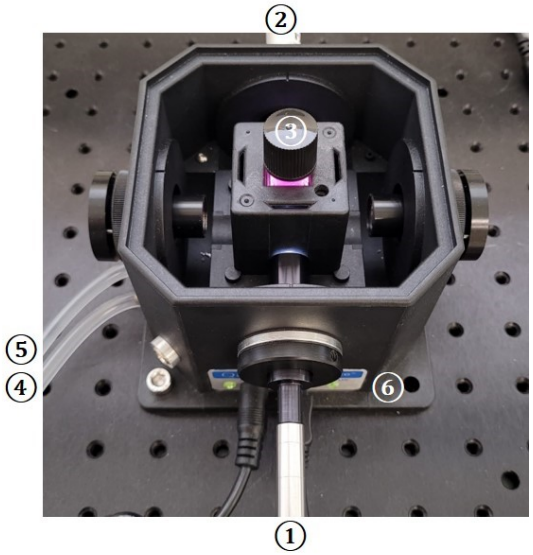

1. Optical fiber input from lamp
2. Output to spectrophotometer
3. Photocatalytic reaction medium
4. Water recirculation inlet
5. Water recirculation outlet
6. Magnetic agitation

Figure S3. Experimental set-up used for the photocatalytic experiments. The use of a recirculation system allows to keep the temperature constant at 20 °C even under prolonged irradiation conditions.

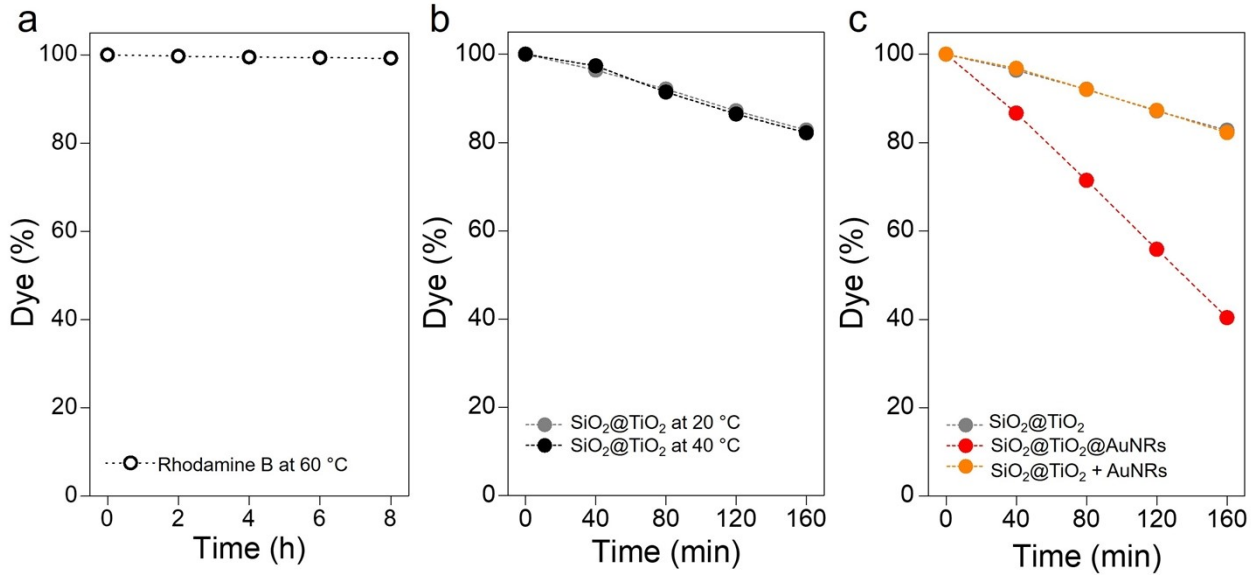

Figure S4. (a) Degradation profile of RhB in water at 60 °C in the dark. (b) Photodegradation profile of RhB in the presence of SiO_2@TiO_2 at 20 °C (dark gray) and 40 °C (black). (c) Photodegradation profile of RhB at 20 °C in the presence of SiO_2@TiO_2 (dark gray), SiO_2@TiO_2 functionalized with 100 nmol of Au NRs (red) and SiO_2@TiO_2 mixed in solution with 100 nmol of Au NRs (orange). The dashed lines are a guide to the eye.

Simulations

Both macroscopic and microscopic models were simulated using COMSOL Multiphysics, a commercial software package implementing finite element methods (FEM) to solve differential equations. The macroscopic model consisted of a glass cuvette, with a 1 cm × 1 cm cross section and 4 cm in height, filled with 4 mL of water and surrounded by air. As described in the main text, we fixed the temperature of the outer lateral walls of the cuvette at T_{room} = 20 °C, reproducing the conditions set by the experimental thermal bath (see above). Moreover, and accounting for the continuous magnetic stirring in the experiment, we simplified the model by spreading the total heat input across the whole body of water. Then, we find the time evolution of the system by solving the heat diffusion equation, in absence of convection and fluid dynamics, using absorption data from the microscopic model and concentration values from the experiment to calculate the amount of heat deposited in the solution.

For the microscopic description of the system, we considered two distinct models: a single Au NR and a SiO_2@AuNRs hybrid. In Figure S5 we present a summary of data from solving the classical electrodynamic response in the frequency domain of these systems under linearly polarized illumination. The spectra of the single Au NR model was obtained by averaging three propagation directions and two orthogonal polarizations, and the hybrid spectra was obtained with a single incidence of light, but randomizing position and orientation of the 36 Au NRs on the surface of SiO_2. The gold permittivity was taken from experimental tables,[7] and the refractive indexes of the different dielectrics were taken as the following constants: $n_{H_2O} = 1.33$, $n_{SiO_2} = 1.45$, and $n_{TiO_2} = 2.5$. The isolated Au NR model was enveloped in a medium with constant permittivity, taken as a weighted average of those of these three materials. The environment of the model for SiO_2@AuNRs is water.

The rates of excitation of hot electrons were computed using a formalism developed in previous publications.[8,9] The following expressions were derived from a quantum-mechanical model of surface-assisted hot electron excitation, and allow the calculation of the rates of excitation of, respectively, all the hot electrons over the Fermi energy, E_F, and hot electrons with energies over a given potential barrier, E_b:

$$Rate_{\mathrm{HE}} = \frac{2}{\pi^2}\frac{e^2 E_{\mathrm{F}}^2}{\mathrm{h}}\frac{1}{(\mathrm{h}\omega)^3}\int_{S_{\mathrm{NC}}} \left|E_{\mathrm{normal}}(\theta,\varphi)\right|^2 \mathrm{d}s$$

$$Rate_{\mathrm{HE},\,\varepsilon>E_{\mathrm{b}}} = \frac{2}{\pi^2}\frac{e^2 E_{\mathrm{F}}^2}{\mathrm{h}}\frac{\mathrm{h}\omega - E_{\mathrm{b}}}{(\mathrm{h}\omega)^4}\int_{S_{\mathrm{NC}}} \left|E_{\mathrm{normal}}(\theta,\varphi)\right|^2 \mathrm{d}s$$

In these expressions, $\hbar\omega$ is the energy of the impinging photons, S_{NC} is the surface of the plasmonic nanocrystal, and E_{normal} is the component of the electric field normal to the surface of the NC immediately inside the material. Lastly, we also present data of the average field enhancement in a volume surrounding the isolated Au NR.

$$FE = \frac{\int_{env} |\mathbf{E}|^2 / E_0^2 \, dV}{\int_{env} dV}$$

Thus, Figure S5c presents the spectrum that illustrates the capabilities of Au NR to enhance optical processes in its environment. As we can see, the enhancement factor is extremely high at the frequency of its longitudinal plasmonic mode. However, this mechanism of energy transfer will be limited to absorption processes occurring around that photon energy, limiting its effectiveness in exciting optical transitions in TiO_2. In contrast, the hot electron excitation spectrum should produce excited carriers capable of being injected in the TiO_2 even at the long-wavelength plasmonic mode (Figure S5b, f).

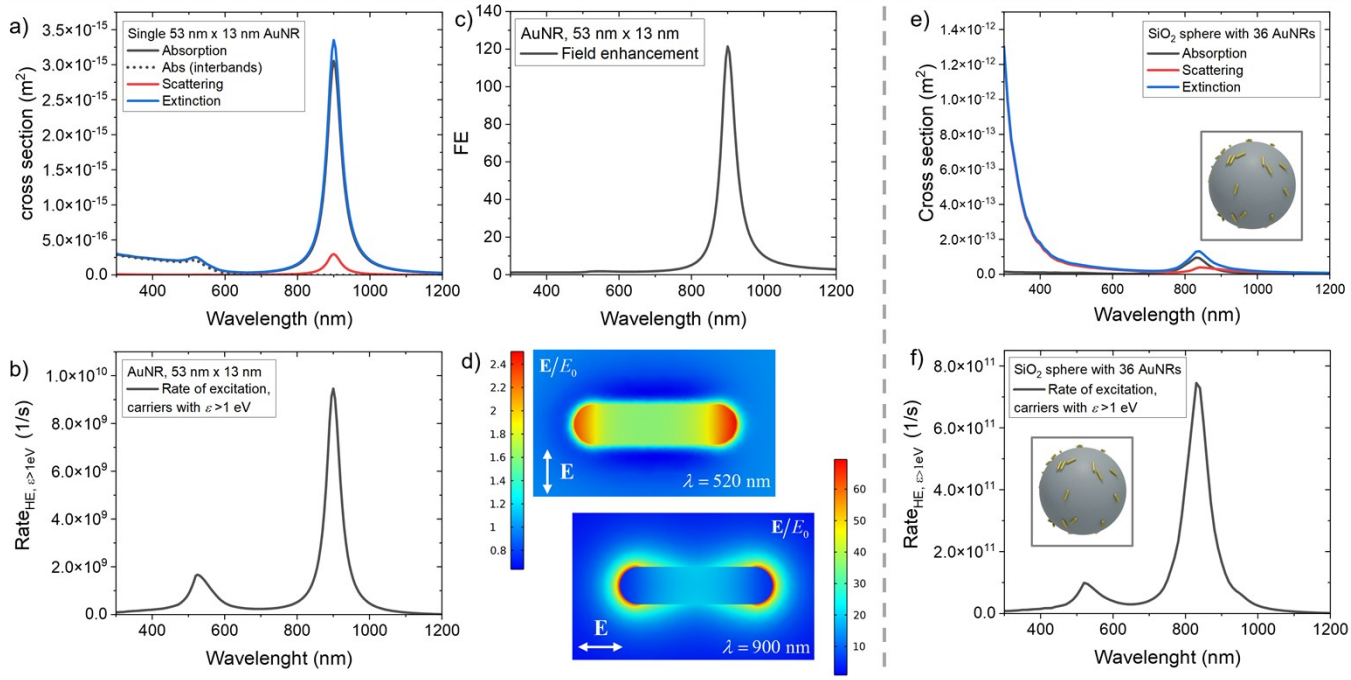

Figure S5. Simulation results for microscopic models: single Au NR (a-d) and SiO_2@AuNRs (e-f). a) Optical interaction cross sections of the Au NR. We also note the contribution of interband transitions to the absorption of the Au NR. (b) Spectrum for the rate of excitation of hot electrons with high energies (above 1 eV over the Fermi level). (c) Total field enhancement around the Au NR. (d) Maps of the enhanced near-field for the two main plasmonic modes of the Au NR. (e) Optical interaction cross sections of a SiO_2 sphere covered with 36 randomly oriented Au NRs. (f) Spectrum for the rate of excitation of hot electrons with high energies over the Au NR ensemble covering the SiO_2 sphere.

Bibliography

(1) Stöber, W.; Fink, A.; Bohn, E. Controlled Growth of Monodisperse Silica Spheres in the Micron Size Range. *J. Colloid Interface Sci.* **1968**, *26*, 62–69.

(2) Scarabelli, L.; Sánchez-Iglesias, A.; Pérez-Juste, J.; Liz-Marzán, L. M. A "Tips and Tricks" Practical Guide to the Synthesis of Gold Nanorods. *J. Phys. Chem. Lett.* **2015**, *6*, 4270–4279.

(3) Pastoriza-Santos, I.; Pérez-Juste, J.; Liz-Marzán, L. M. Silica-Coating and Hydrophobation of CTAB-Stabilized Gold Nanorods. *Chem. Mater.* **2006**, *18*, 2465–2467.

(4) Leichnitz, S.; Heinrich, J.; Kulak, N. A Fluorescence Assay for the Detection of Hydrogen Peroxide and Hydroxyl Radicals Generated by Metallonucleases. *Chem. Commun.* **2018**, *54*, 13411–13414.

(5) Entradas, T.; Waldron, S.; Volk, M. The Detection Sensitivity of Commonly Used Singlet Oxygen Probes in Aqueous Environments. *J. Photochem. Photobiol. B Biol.* **2020**, *204*, 111787.

(6) Nosaka, Y.; Nosaka, A. Y. Generation and Detection of Reactive Oxygen Species in Photocatalysis. *Chem. Rev.* **2017**, *117*, 11302–11336.

(7) Johnson, P. B.; Christy, R. W. Optical Constants of the Noble Metals. *Phys. Rev. B* **1972**, *6*, 4370–4379.

(8) Besteiro, L. V.; Kong, X.-T.; Wang, Z.; Hartland, G.; Govorov, A. O. Understanding Hot-Electron Generation and Plasmon Relaxation in Metal Nanocrystals: Quantum and Classical Mechanisms. *ACS Photonics* **2017**, *4*, 2759–2781.

(9) Santiago, E. Y.; Besteiro, L. V.; Kong, X.-T.; Correa-Duarte, M. A.; Wang, Z.; Govorov, A. O. Efficiency of Hot-Electron Generation in Plasmonic Nanocrystals with Complex Shapes: Surface-Induced Scattering, Hot Spots, and Interband Transitions. *ACS Photonics* **2020**, *7*, 2807–2824.